Beyond Quadtrees: Cell Decompositions for Path Planning using Wavelet Transforms

Raghvendra V. Cowlagi and Panagiotis Tsiotras

Abstract— Path planning techniques based on hierarchical multiresolution cell decompositions are suitable for online implementation due to their simplicity and speed of implementation. We present an efficient multiresolution cell decomposition scheme based on the Haar wavelet transform. The decomposition approximates the environment using high resolution close to the agent and coarse resolution elsewhere. We demonstrate an algorithm to extract the adjacency and transition cost relations of the cells directly from the wavelet transform coefficients.

I. INTRODUCTION

The problem of planning a path for an autonomous mobile robot in a given workspace, while avoiding obstacles, has been studied for several years (see [1], [2], and more recently, [3]). Solution methods fall into three broad categories: cell decomposition, roadmap methods, and artificial potential field methods. The first two approaches transform the path planning problem into a graph search problem. In particular, cell decomposition methods partition the free space into convex, non-overlapping regions, called cells, and then employ techniques, such as the Dijkstra algorithm, to search the connectivity graph for a sequence of adjacent cells from the initial point to the goal [1, Ch. 5 and 6]. Exact cell decomposition methods create partitions such that the union of cells is equal to the free space. Approximate methods decompose the free space into cells of simple shapes, usually rectangles, and classify them as FREE or FULL, based on whether they belong to the free space or obstacle space respectively. Iterative decomposition schemes classify cells obtained in intermediate iterations as MIXED if they intersect both the obstacle space and the free space. Hierarchical path planning techniques may allow paths to travel through MIXED cells and refine them in subsequent iterations [4], [5], [6]. The iterations continue until all MIXED cells are decomposed into FREE or FULL cells. One of the most extensively used approximate cell decomposition techniques is the quadtree method [4], [7], [8], which employs recursive decompositions of MIXED cells into four square subcells (children) until all cells are either FREE or FULL.

Although several sophisticated approaches for path planning have been reported in the literature, approaches based on cell decompositions of the environment are most common and are widely used in applications because of their simplicity. Note that it is also advantageous to decompose the free space into as few cells as possible, in order to make search of the corresponding graph faster. Working with multiresolution cell decompositions is beneficial when one is primarily interested in online implementation. A multiresolution scheme can keep the size of the resulting graph search tractable so that its search can be achieved with the limited on-board computational resources, while keeping the required accuracy. Multiresolution schemes have been proposed recently by Behnke [6] and Tsiotras [9]. Hwang *et al* [10] describe a multiresolution technique using triangles, instead of rectangles, as cells. Other implementations of multiresolution techniques include Prazenica *et al* [11], who present a model-predictive (receding horizon) control formulation of the path planning problem using multiresolution estimates of object locations; Kim and Lee [12] present a multiresolution potential field approach to path planning; and Verwer [13] describes the use of a hierarchy of imaginary spheres encapsulating the robot for collision avoidance.

In this paper, we propose the use of wavelet transforms in order to perform fast cell decomposition with varying levels of resolution. The application of the wavelet transform to path planning has been studied in the past, albeit in a somewhat different context than our work. Pai and Reissell [5] present an algorithm for path planning over a rough terrain. They iteratively refine the path based on successively finer approximations of the terrain elevation map. At each iteration, the wavelet transform coefficients of the elevation map are used to compute the approximation errors, which are then included in the cost function that should be minimized by the optimal path. Sinopoli *et al* [14] describe a similar approach for vision-based path planning for autonomous UAVs. Carrioli [15] describes the use of the Haar wavelet for reducing computations, while manipulating images representing the environment. In a slightly different application, Narayanswami and Pang [16] describe a path planning algorithm for NC machining that uses successively finer approximations to the required contour as the cutting tool approaches the contour.

The common characteristic of most previous works is that they employ the multiresolution approximation property of the wavelet transform *sequentially*, that is, the path planning algorithm is executed over several iterations. At each iteration the resolution is increased and/or the searched area of the workspace is reduced accordingly. Each iteration thus results in a refinement of the path obtained in the previous iteration. In this paper, we revisit the multiresolution decomposition scheme of [9] that represents different

regions of the workspace at different resolutions *simultaneously*. In [9] the authors demonstrate the effectiveness of a wavelet-based decomposition scheme in which the robot's immediate environment is approximated finely, while the distant locations coarsely so. In particular, we complement the work in [9] by presenting an algorithm for computing the adjacency and transition cost matrices directly from the wavelet decomposition. It is shown that, as expected, this speeds up the whole path-planning process.

The rest of the paper is organized as follows: Section II provides a brief introduction to the discrete wavelet transform, while concentrating on its application to multiresolution cell decomposition. The reader is referred to [17], [18], and [19] for more detailed expositions on the mathematical theory of the wavelet transform. Section III describes the computation of the locations, dimensions, and average intensities of the cells using the information provided by the nonzero wavelet detail coefficients. Section IV presents sample results of the proposed method, along with a comparison against the standard quadtree decomposition.

II. CELL DECOMPOSITION USING WAVELETS

A. The Wavelet Transform

The discrete wavelet transform provides a framework for multiresolution analysis (MRA) of a function, that is, the construction of a hierarchy of functional approximations by projecting the function onto a sequence of nested linear spaces. Such a sequence of nested linear spaces is generated by translated and scaled versions of two functions $\phi : \mathbb{R} \to \mathbb{R}$ and $\psi : \mathbb{R} \to \mathbb{R}$ of unit energy, called the *scaling function* and *wavelet* respectively, satisfying the *orthogonality equations*

$$
\begin{aligned}
\langle \phi(t), \phi(t-n) \rangle &= \delta(n), & (1) \\
\langle \psi(t), \psi(t-n) \rangle &= \delta(n), & (2) \\
\langle \psi(t), \phi(t-n) \rangle &= 0. & (3)
\end{aligned}
$$

where $\langle \cdot, \cdot \rangle$ denotes the inner product, and such that there exist sequences $h(n)$ and $g(n)$ of scalars satisfying the following relations, known as the *dilation equations*

$$
\phi(t) = \sum_{n=-\infty}^{\infty} h(n)\phi(2t-n), \qquad (4)
$$

$$
\psi(t) = \sum_{n=-\infty}^{\infty} g(n)\phi(2t-n). \qquad (5)
$$

Defining V_j as the linear space spanned by $\{\phi_{j,k}\} \stackrel{\text{def}}{=} \{\sqrt{2}^j \phi(2^j t - k) : k \in \mathbb{Z}\}$, it can be shown (see, for instance, [17, Ch. 3]) that $\{V_j\}_{j \in \mathbb{Z}}$ is a sequence of nested subspaces, such that $\dots V_{-1} \subset V_0 \subset V_1 \dots$; that $\overline{\bigcup V_j} = \mathscr{L}^2(\mathbb{R})$, $j \in \mathbb{Z}$; and that $\{\psi_{j,k}\} \stackrel{\text{def}}{=} \{\sqrt{2}^j \psi(2^j t - k) : k \in \mathbb{Z}\}$ is a basis set for $W_j \stackrel{\text{def}}{=} V_j \backslash V_{j-1}$. The discrete wavelet transform of a function $f : \mathbb{R} \to \mathbb{R}$, $f \in \mathscr{L}^2(\mathbb{R})$, may be written as

$$
c_{j_0,k} = \langle \phi_{j_0,k}(t), f(t) \rangle, \qquad d_{j,k} = \langle \psi_{j,k}(t), f(t) \rangle.
$$

The corresponding reconstruction equation is

$$
f(t) = \sum_{k=-\infty}^{\infty} c_{j_0,k}\phi_{j_0,k}(t) + \sum_{j=j_0}^{\infty}\sum_{k=-\infty}^{\infty} d_{j,k}\psi_{j,k}(t).
$$

The scalars $c_{j_0,k}$ and $d_{j,k}$ are known as *approximation* and *detail* coefficients respectively. The first term in (6) is the approximation of $f(t)$ at *resolution* j_0, while the inner summation of the second term is the difference between approximations at two successive levels of resolution.

The simplest example of scaling and approximation functions is the Haar family, defined as

$$
\phi(t) \stackrel{\text{def}}{=} \begin{cases} 1 & 0 \le t < 1 \\ 0 & \text{otherwise} \end{cases} , \quad \psi(t) \stackrel{\text{def}}{=} \begin{cases} 1 & 0 \le t < 1/2 \\ -1 & 1/2 \le t < 1 \\ 0 & \text{otherwise.} \end{cases}
$$

(6)

For the Haar family, V_j corresponds to the set of piecewise-constant functions over the regularly spaced intervals $\mathscr{I}_{j,k} \stackrel{\text{def}}{=} [2^{-j}k, 2^{-j}(k+1)]$ of length 2^{-j}. The approximation coefficient $c_{j,k}$, at a given resolution j, is equal to the average value of the function over the kth interval.

The two-dimensional wavelet transform is a simple extension of the 1-D transform presented above. The scaling and wavelet functions for the 2-D case are defined as

$$
\begin{aligned}
\Phi_{j,k,\ell}(x,y) &= \phi_{j,k}(x)\phi_{j,\ell}(y), & (7) \\
\Psi^1_{j,k,\ell}(x,y) &= \phi_{j,k}(x)\psi_{j,\ell}(y), & (8) \\
\Psi^2_{j,k,\ell}(x,y) &= \psi_{j,k}(x)\phi_{j,\ell}(y), & (9) \\
\Psi^3_{j,k,\ell}(x,y) &= \psi_{j,k}(x)\psi_{j,\ell}(y). & (10)
\end{aligned}
$$

The linear spaces V_j are now defined as the span of $\{\Phi_{j,k,\ell}(x,y) : k,\ell \in \mathbb{Z}\}$ and the difference $V_j \backslash V_{j-1}$ is represented as the union of three mutually orthogonal spaces $W_j^{\text{h}}, W_j^{\text{v}}, W_j^{\text{d}}$, which are the spans of translations of the three wavelet functions $\Psi^1_{j,k,\ell}(x,y), \Psi^2_{j,k,\ell}(x,y)$, and $\Psi^3_{j,k,\ell}(x,y)$, respectively. Thus, the discrete wavelet transform of a function $f : \mathbb{R}^2 \to \mathbb{R}$, $f \in \mathscr{L}^2(\mathbb{R}^2)$ is

$$
c_{j_0,k,\ell} = \langle \Phi_{j,k,\ell}(x,y), f(x,y) \rangle, \quad d^i_{j,k,\ell} = \langle \Psi^i_{j,k,\ell}(x,y), f(x,y) \rangle,
$$

and the reconstruction equation is

$$
\begin{aligned}
f(x,y) = &\sum_{k,\ell=-\infty}^{\infty} c_{j_0,k,\ell}\Phi_{j,k,\ell}(x,y) + \\
&\sum_{i=1}^{3}\sum_{j=j_0}^{\infty}\sum_{k,\ell=-\infty}^{\infty} d^i_{j,k,\ell}\Psi^i_{j,k,\ell}(x,y). \quad (11)
\end{aligned}
$$

B. Application to Cell Decompositions

An *image* of the environment is a compact, square region $\mathscr{R} \subset \mathbb{R}^2$ with an associated intensity map $\mathscr{F} : \mathscr{R} \to \mathbb{R}$. In the context of path planning, the image could represent an elevation map of the terrain on which the robot is to move, or a risk measure that represents the probability that the corresponding location is occupied by an obstacle [9].

Let the coarse resolution level j_0 be given, and let $a_{j_0,k,\ell}$ and $d^i_{j,k,\ell}$ be the two-dimensional discrete wavelet transform coefficients of the intensity map of the image $\mathscr{F}$. Let $\mathscr{A}_{j_0} \stackrel{\text{def}}{=} \{(j_p, k_p, \ell_p)\}$ be a set of triplets of integers such that $j_p \ge j_0$, $p = 0, 1, 2, \dots$. An *approximation* of $\mathscr{F}$, say $\hat{\mathscr{F}}$, is any image obtained by the reconstruction of $a_{j_0,k,\ell}$ and $\hat{d}^i_{j,k,\ell}$, where

$$
\hat{d}^i_{j,k,\ell} = \begin{cases} d^i_{j,k,\ell} & i=1,2,3; \ (j,k,\ell) \in \mathscr{A}_{j_0} \\ 0 & \text{otherwise.} \end{cases}
$$

In the rest of this paper, we denote an approximate image by its associated set of non-zero detail coefficients $\mathscr{A}_{j_0}$, in a minor abuse of notation.

A cell decomposition of the environment is achieved through an appropriate selection of $\mathscr{A}_{j_0}$, along with the use of a compactly supported scaling function and wavelet. The Haar wavelet and the Daubechies, symlet, and coiflet families of wavelets [20] are all examples of compactly supported wavelets. Since the scaling function $\phi_{j,k}$ and wavelet $\psi_{j,k}$ are supported over the interval $\mathscr{I}_{j,k}$, the corresponding 2-D functions, defined in (7)-(10), are supported over the rectangle $\mathscr{C}_{j,k,\ell} \stackrel{\text{def}}{=} \mathscr{I}_{j,k} \times \mathscr{I}_{j,\ell}$, known as a *cell*.

Consider the 2-D Haar scaling function and wavelets in (7)-(10). The approximation of the environment at resolution j_0, namely, its projection on to the linear space V_{j_0}, is a linear combination of the basis $\{\Phi_{j_0,k,\ell}(x,y) : k,\ell \in \mathbb{Z}\}$. For instance, the approximation at resolution j_0 is the first term in the right-hand-side of (11). Clearly, such an approximation is piecewise constant over the cell decomposition $\mathscr{P}_{j_0} = \{\mathscr{C}_{j_0,k,\ell} : \bigcup_{k,\ell \in \mathbb{Z}} \mathscr{C}_{j_0,k,\ell} = \mathscr{R}\}$. The intensity of the approximation over a cell is the average intensity over the area of the cell. It is possible to construct a *multiresolution approximation*, $\mathscr{P}^{\mu}_{j \geq j_0}$ by first constructing an approximation at resolution j_0, and then successively expressing Φ_{j,k_j,ℓ_j}, for some pairs (k_j,ℓ_j), as a linear combination of $\{\Phi_{j+1,k_{j+1},\ell_{j+1}}(x,y) : k_{j+1},\ell_{j+1} \in \mathbb{Z}\}$, similar to (5) for the 1-D case. A multiresolution approximation is a piecewise constant function over a cell decomposition in which cells are of different dimensions at different location, that is, $\mathscr{P}^{\mu}_{j \geq j_0} = \{\mathscr{C}_{j,k,\ell} : \bigcup_{j,k,\ell} \mathscr{C}_{j,k,\ell} = \mathscr{R}, \; j \geq j_0, \; k \in K(j), \; \ell \in L(j)\}$, where $K(j)$ and $L(j)$ are some resolution-dependent index subsets of $\mathbb{Z}$.

In Ref. [9] the authors describe path planning algorithm based on multiresolution cell decomposition arising from the 2-D wavelet transform.

Figure 1 shows an example of the original environment of dimension 16×16 pixels, and its approximation with the following data (coarsest level $j_0 = 2$):

$$\begin{aligned} \mathscr{A}_{j_0} = & \{(2,0,2),(2,3,2),(3,3,4),(3,4,2),(3,4,3), \\ & (3,5,2),(3,6,5)\}. \end{aligned} \tag{12}$$

III. ADJACENCY MATRIX

In this section we present a scheme for determining all elements of the cell decomposition $\mathscr{P}^{\mu}_{j \geq j_0}$ and their intensities for a given approximation $\mathscr{A}_{j_0}$, for the Haar system directly from the wavelet transform coefficients. The corresponding adjacency matrix may then be computed using off-the-shelf code.

A. Cell Locations and Dimensions

We note that the Haar scaling function defined in (6) satisfies the following dilation equation [17, Sec. 2.3.2]

$$\phi(t) = \phi(2t) + \phi(2t-1) \tag{13}$$

Since $\phi(t)$ is defined over the closed unit interval, supports of its translations do not overlap with each other, a property
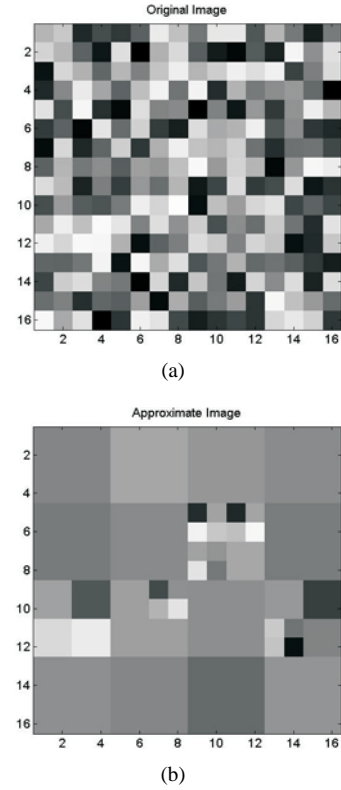

(a)

(b)

Fig. 1. Example of an image and its approximation

which also holds true for the corresponding 2-D scaling function. Further, (13) implies that the support of $\phi_{j,k}(t)$ is exactly equal to the union of the supports of $\phi_{j+1,k}(t)$ and $\phi_{j+1,k-1}(t)$. In the 2-D case, this corresponds to a square support of $\Phi_{j,k,\ell}(t)$ being exactly equal to the union of the supports of $\Phi_{j+1,k,\ell}(t)$, $\Phi_{j+1,k-1,\ell}(t)$, $\Phi_{j+1,k,\ell-1}(t)$, and $\Phi_{j+1,k-1,\ell-1}(t)$. If the detail coefficients at level j and at finer levels $j+1, j+2, \ldots$ are all zero, then $c_{j,k,\ell}\Phi_{j,k,\ell}(t)$ represents the finest available approximation of the image over that particular region of support, where $c_{j,k,\ell}$ is the corresponding approximation coefficient. If any of the three detail coefficients at level j is non-zero, then a finer approximation is possible. For the Haar wavelet system, this is equivalent to a decomposition of the cell $\mathscr{C}_{j,k,\ell}$ into the cells $\{\mathscr{C}_{j+1,\hat{k},\hat{\ell}} : k-1 \leq \hat{k} \leq k, \; \ell-1 \leq \hat{\ell} \leq \ell\}$.

Since the translations of the wavelet and scaling functions are orthogonal to each other, one may associate the detail coefficients with specific regions in $\mathbb{R}^2$, such that the values of those coefficients affect the approximate image only in that region. For the Haar system, due to the dilation equation (13), we can make the following association

$$\begin{aligned} d^i_{j,k,\ell} \longleftrightarrow & \{(x,y) \in \mathbb{R}^2 : 2^{j_0}X_k \leq x < 2^{j_0}(X_k+1), \\ & 2^{j_0}Y_\ell \leq y < 2^{j_0}(Y_\ell+1)\} \end{aligned} \tag{14}$$

where $X_k = \lfloor 2^{j_0-j}k \rfloor$ and $Y_\ell = \lfloor 2^{j_0-j}\ell \rfloor$. The reason for making this association will become apparent once the rules for computing the elements of $\mathscr{P}^{\mu}_{j \geq j_0}$ are detailed later on. Roughly speaking, if coefficients at a finer level are non-zero, while all the coarser-level coefficients associated with
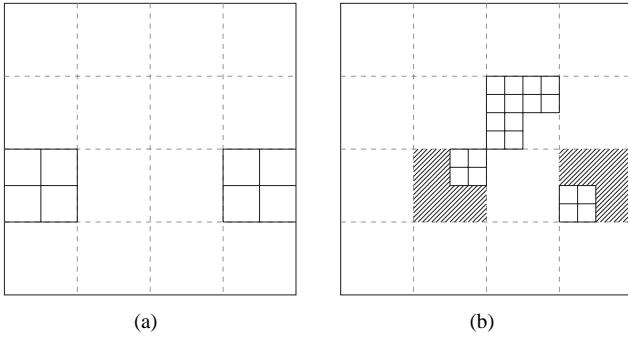
Fig. 2. (a) Rule 2) applied to level 2 coefficients, along with Rule 1); (b) Rule 2) applied to level 1 coefficients.
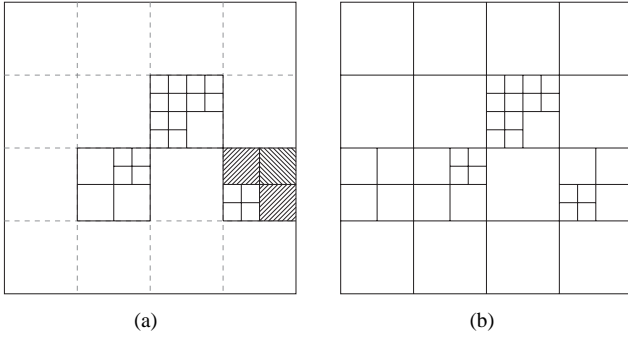

Fig. 3. (a) Rule 3) applied to level 1 coefficients; (b) Resultant cell decomposition.

the same region are zero, a non-convex cell may result (see, for instance, Fig. 2)(b). Any non-convex cells must be decomposed further into cells of coarser resolutions.

We can formulate the following Rules upon which the algorithm for determining the elements of $\mathscr{P}^{\mu}_{j \geq j_0}$ are based. If $(j, k, \ell) \in \mathscr{A}_{j_0}$, then:

Rule 1) $\{\mathscr{C}_{j_0, \hat{k}, \hat{\ell}} : 0 \leq \hat{k}, \hat{\ell} \leq 2^{j_0 - p} - 1\} \in \mathscr{P}^{\mu}_{j \geq j_0}$, where $p = \log_2 N$, and N is the number of pixels in each row or column of the image. When all the detail coefficients are neglected, these cells form a uniform grid due to the approximation coefficients alone.

Rule 2) $\{\mathscr{C}_{j+1, \hat{k}, \hat{\ell}} : 2k \leq \hat{k} \leq 2k + 1, \ 2\ell \leq \hat{\ell} \leq 2\ell + 1\} \in \mathscr{P}^{\mu}_{j \geq j_0}$. This is a consequence of the fact that the support of the Haar scaling function at a given level is equal to the union of the four supports of those at the next finer level.

Rule 3) $\{\mathscr{C}_{j+1, \hat{k}, \hat{\ell}} : \hat{X}_{\hat{k}} - 1 \leq \hat{k} \leq \hat{X}_{\hat{k}}, \ \hat{Y}_{\hat{\ell}} - 1 \leq \hat{\ell} \leq \hat{Y}_{\hat{\ell}}, \ j_0 \leq \hat{j} < j\} \in \mathscr{P}^{\mu}_{j \geq j_0}$, where $\hat{X}_{\hat{k}} = \lfloor 2^{\hat{j} - j} k \rfloor$ and $\hat{Y}_{\hat{\ell}} = \lfloor 2^{\hat{j} - j} \ell \rfloor$. This rule is required to account for the need to decompose non-convex cells, which may arise when a finer level coefficient is non-zero, while coarser coefficients associated with the same region, as given by (14) are zero.

Rule 4) $\{\mathscr{C}_{\hat{j}, \hat{k}, \hat{\ell}} : \hat{k} = \lfloor 2^{\hat{j} - j} k \rfloor, \ \hat{\ell} = \lfloor 2^{\hat{j} - j} \ell \rfloor, \ j_0 \leq \hat{j} \leq j\} \notin \mathscr{P}^{\mu}_{j \geq j_0}$. This rule simply indicates that once a cell $\mathscr{C}_{j, k, \ell}$ is decomposed, it cannot belong to $\mathscr{P}^{\mu}_{j \geq j_0}$.

Clearly, Rules 3) and 4) conflict with each other since

some cells that are prescribed by Rule 3) for inclusion in $\mathscr{P}^{\mu}_{j \geq j_0}$, are also prescribed for exclusion by Rule 4). Furthermore, Rules 2) and 3) prescribe some of the same cells for inclusion in $\mathscr{P}^{\mu}_{j \geq j_0}$. The algorithm for determining elements of $\mathscr{P}^{\mu}_{j \geq j_0}$ must hence account for this conflict and possible redundancy. In particular, the redundancy may be avoided by checking for non-zero coefficients at higher (coarser) levels associated with the same region, as given by the association (14).

B. Cell Values

In order to calculate the cell intensities, we use the single-step reconstruction equation for the Haar wavelet repeatedly:

$$[a_{j+1, \hat{k}, \hat{\ell}}] = 2^{j - j_0} \begin{bmatrix} 1 & 1 & 1 & 1 \\ 1 & -1 & 1 & -1 \\ 1 & 1 & -1 & -1 \\ 1 & -1 & -1 & 1 \end{bmatrix} \begin{bmatrix} c_{j,k,\ell} \\ d^1_{j,k,\ell} \\ d^2_{j,k,\ell} \\ d^3_{j,k,\ell} \end{bmatrix}, \quad (15)$$

where $a_{\hat{k}, \hat{\ell}}$ are the intensities of the cells $\{\mathscr{C}_{j+1, \hat{k}, \hat{\ell}} : 2k \leq \hat{k} \leq 2k + 1, \ 2\ell \leq \hat{\ell} \leq 2\ell + 1\}$, $c_{j,k,\ell}$ is the approximation coefficient, while $d^i_{j,k,\ell}$, $i = 1, 2, 3$ are the detail coefficients.

The intensities of cells arising from Rule 1) are given by $a_{j_0, k, \ell} = 2^{j_0} c_{j_0, k, \ell}$. When a non-zero coefficient at level j is detected, the largest index $j_1 < j$ associated with the same region, as given by (14), is determined and the intensities of the cells arising from Rule 2) are calculated using (15). The intensities of cells arising from each application of Rule 3) are the same, and are inherited from a previous application of (15) that corresponds to the non-zero detail coefficients (associated with the same region) of the finest level of resolution that this coarser than the current one.

IV. EXAMPLES

Figures 2 and 3 illustrate the application of these Rules for the example given in (12). Figure 2(a) shows the grid due to the approximation coefficients alone, and the cells due to the non-zero coefficients at the coarsest level, i.e., $j = 2$. The shaded cells in Fig. 2(b) illustrate the non-convex regions that may arise due to non-zero coefficients at finer levels, which need to be decomposed using Rule 3). The shaded cells in Fig. 3(a) are those which arise twice: due to Rule 2) for level $j = 2$ coefficients and due to Rule 3) for level $j = 3$ coefficients. Figure 3(b) shows the final cell decomposition, which should be compared with the actual reconstructed approximate image in Fig. 1(b).

Figures 4 and 5 illustrate an implementation of wavelet-based multiresolution path planning using the algorithm proposed in this paper. The initial point and goal are indicated by a square and diamond respectively. The image shown in the figures corresponds to terrain height, where the red shades indicate low terrain (favorable), and blue shades indicate high terrain (unfavorable). The cost function used was a weighted sum of terrain height and distance traveled. Figure 4(a) shows the initial multiresolution approximation of the intensity map with high resolution near the initial point, while Fig. 4(b) shows the final path computed. It can be seen that the path remains in the darker shades

of red throughout. Figure 5 shows an intermediate step of multiresolution approximation with high resolution near the current position of the agent, while Fig. 5 shows the history of the path traversed by the agent until that point. The original intensity map considered was of resolution 512×512 pixels. Whilst using this resolution throughout would have given a cell decomposition with more than 250,000 nodes, the multiresolution algorithm gives a decomposition with only around 400 nodes in each iteration.
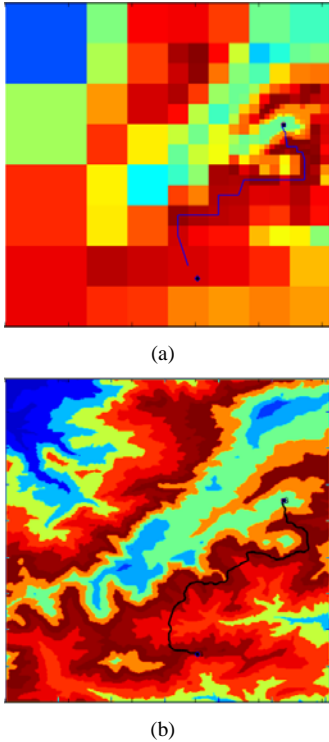

(a)

(b)

Fig. 4.   Multi-resolution path planning

Figure 6 shows another example of an image $(N = 32)$ and its approximation, with the cell decomposition superimposed for comparison. The following approximation has been used, with $j_0 = 4$:

$$\mathscr{A}_{j_0} = \{(1,0,1),(2,1,2),(3,2,4),(3,2,5),(3,3,5),$$
$$(4,7,11),(4,8,11)\}$$

Note that, in the "fourth quadrant" region $\{(x,y) \in \mathbb{R}^2 : 16 \leq x < 32, \ 16 \leq y < 32\}$, only one coefficient, *viz.* $(4,8,11)$ is non-zero. Since this coefficient is at the finest resolution, it necessitates cells of higher dimensions too, as shown.

Table I shows a comparison of execution times for the computation of the adjacency matrix against the quadtree method. The proposed algorithm shows an improvement of roughly 30% to 40%, which is significant, since this savings occurs at each iteration. Table I was obtained by executing the code on the following family of approximate images:

$$\mathscr{A}_{j_0} = \{(j,k,\ell) : \lfloor \frac{q_1}{2^j} \rfloor - \delta \leq k \leq \lfloor \frac{q_1}{2^j} \rfloor + \delta,$$
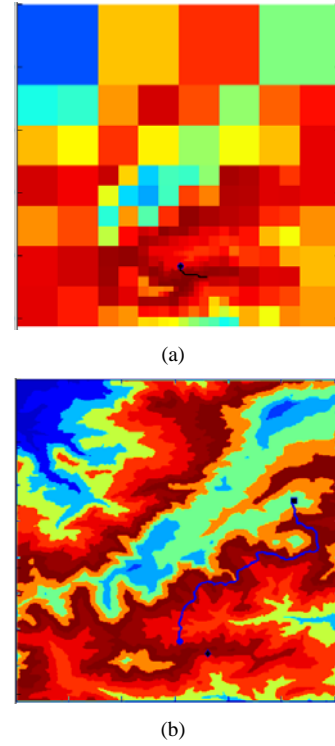$$\lfloor \frac{q_2}{2^j} \rfloor - \delta \leq \ell \leq \lfloor \frac{q_2}{2^j} \rfloor + \delta, \ N \geq j \geq j_0\}$$

(a)

(b)

Fig. 5.   Intermediate step in path planning

TABLE I

SAMPLE RESULTS

p	j_0	Nodes	Quadtree $t(s)$	Wavelet $t(s)$	Difference (%)
3	2	35	0.0297	0.0115	61.40
3	0	34	0.0208	0.0083	60.00
4	1	54	0.0224	0.0125	44.19
6	5	1050	0.0723	0.0641	11.51
7	2	139	0.1010	0.0718	28.87
7	1	135	0.1016	0.0755	25.64
8	4	357	0.3411	0.2307	32.37
9	5	1129	1.4281	0.9505	33.44
10	3	238	5.8844	4.4078	25.09
11	5	1181	23.917	16.502	31.01

where $(q_1, q_2) \in [0, N-1] \times [0, N-1]$ is an random point on the image. The decomposition is such that the approximate image resembles the original image accurately around (q_1, q_2) and coarsely away from it, and $\delta \in \mathbb{N}$ is a parameter. In the results of Table I the value of $\delta = 3$ has been used.

V. CONCLUSIONS

In this paper we have proposed a computationally efficient algorithm for constructing the connectivity matrix of cell decompositions, and the associated intensity map arising from multiresolution approximations of the environment using wavelet transforms. In particular, we have shown that one is able to compute the connectivity (adjacency) matrix of the cells directly from the discrete wavelet transform, thus bypassing the direct computation of quadtree decompositions. Numerical examples confirm that the proposed approach provides advantages in terms of computer memory and speed. Wavelet-based cell decompositions thus offer a
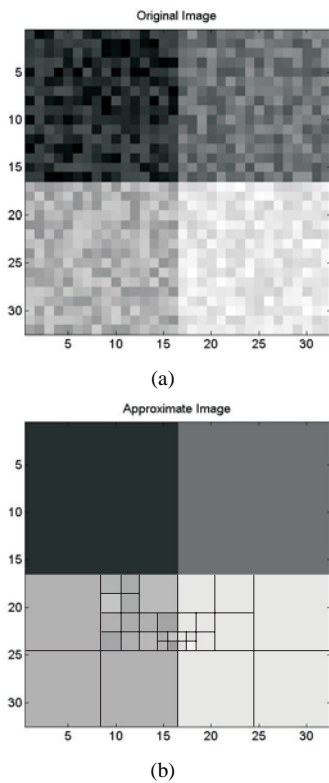
Fig. 6. Example of an image and its approximation

computationally attractive alternative to quadtrees for on-line path planning problems.

REFERENCES

[1] J.-C. Latombe, *Robot Motion Planning*. Kluwer Academic Publishers, 1991.

[2] Y. K. Hwang and N. Ahuja, "Gross motion planning - a survey," *ACM Computing Surveys*, vol. 24, no. 3, pp. 219–291, September 1992.

[3] S. M. LaValle, *Planning Algorithms*. Cambridge University Press, 2006.

[4] S. Kambhampati and L. S. Davis, "Multiresolution path planning for mobile robots," *IEEE J. Robotics and Automation*, vol. RA-2, no. 3, pp. 135–45, September 1986.

[5] D. K. Pai and L.-M. Reissell, "Multiresolution rough terrain motion planning," *IEEE Trans. Robotics & Automation*, vol. 14, no. 1, pp. 19–33, February 1998.

[6] S. Behnke, "Local multiresolution path planning," *Lecture Notes in Artificial Intelligence*, vol. 3020, pp. 332–43, 2004.

[7] H. Samet, "The quadtree and related hierarchical data structures," *Computing Surveys*, vol. 16, no. 2, pp. 187–260, June 1984.

[8] H. Noborio, T. Naniwa, and S. Arimoto, "A quadtree-based path planning algorithm for a mobile robot," *Journal of Robotic Systems*, vol. 7, no. 4, pp. 555–74, 1990.

[9] P. Tsiotras and E. Bakolas, "A hierarchical on-line path planning scheme using wavelets," in *to appear, European Control Conference*, 2007.

[10] J. Y. Hwang, J. S. Kim, S. S. Lim, and K. H. Park, "A fast path planning by path graph optimization," *IEEE Trans. Systems, Man, and Cybernetics*, vol. 33, no. 1, pp. 121–127, January 2003.

[11] R. J. Prazenica, A. J. Kurdila, R. C. Sharpley, and J. Evers, "Multiresolution and adaptive path planning for maneuver of micro-air-vehicles in urban environments," *AIAA Guidance, Navigation, and Control Conference and Exhibit*, 2005.

[12] C.-T. Kim and J.-J. Lee, "Mobile robot navigation using multi-resolution electrostatic potential field," in *32nd Annual Conference of IEEE Industrial Electronics Society, 2005, IECON 2005*, 2005.

[13] B. J. H. Verwer, "A multiresolution workspace, multiresolution configuration space approach to solve the path planning problem," in *Proc. 1990 IEEE Intl. Conf. Robotics & Automation*, 1990, pp. 2107–12.

[14] B. Sinopoli, M. Micheli, G. Donato, and T. J. Koo, "Vision based navigation for an unmanned aerial vehicle," in *Proc. 2001 IEEE Conf. Robotics & Automation*, 2001, pp. 1757–64.

[15] L. Carrioli, "Unsupervised path planning of many asynchronously self-moving vehicles," in *IEEE/RSJ Intl. Workshop on Intelligent Robots and Systems IROS '91*, 1991, pp. 555–59.

[16] R. Narayanaswami and J. Pang, "Multiresolution analysis as an approach for tool path planning in nc machining," *Computer-Aided Design*, vol. 35, pp. 167–78, 2003.

[17] R. M. Rao and A. S. Bopardikar, *Wavelet Transforms - Introduction to Theory and Applications*. Addison-Wesley, 1998.

[18] S. G. Mallat, "A theory for multiresolution signal decomposition: The wavelet representation," *IEEE Trans. Pattern Analysis and Machine Intelligence*, vol. 11, no. 7, pp. 674–93, 1989.

[19] C. S. Burrus, R. A. Gopinath, and H. Guo, *Introduction to Wavelets and Wavelet Transforms - A Primer*. Prentice Hall, 1998.

[20] I. Daubechies, *Ten Lectures on Wavelets*. CBMS-NSF Lecture Notes, 61, SIAM, 1994.